NOLTA, IEICE

Paper

Quantifying smoothing effects of wind power via Koopman mode decomposition: A numerical test with wind speed predictions in Japan

Fredrik Raak [1a)], *Yoshihiko Susuki* [2b)], *Kazuhisa Tsuboki* [3], *Masaya Kato* [3], *and Takashi Hikihara* [1]

[1] *Department of Electrical Engineering, Kyoto University*
Nishikyo, Kyoto 615–8510, Japan

[2] *Department of Electrical and Information Systems, Osaka Prefecture University*
1–1 Gakuen-cho, Naka-ku, Sakai 599–8531, Japan

[3] *Hydrospheric-Atmospheric Research Center, Nagoya University*
Chikusa, Nagoya 464–8601, Japan

[a)] *f-raak@dove.kuee.kyoto-u.ac.jp*
[b)] *susuki@eis.osakafu-u.ac.jp*

Received September 19, 2016; Revised March 29, 2017; Published October 1, 2017

Abstract: Wind power has increased rapidly worldwide in recent years. For power system and wind farm operators, it becomes important to understand the smoothing effects of aggregated power, and the temporal and spatial scales at which smoothing is achieved. Here, we propose a new smoothing index for wind power based on the so-called Koopman Mode Decomposition (KMD). KMD decomposes spatio-temporal data on complex wind power into modes oscillating with single frequencies. We show that the proposed smoothing index is regarded as a generalization of a previously proposed index based on power spectral densities. We then look at smoothing of wind power in Japan on a large-scale by incorporating highly-resolved wind prediction data from the Cloud Resolving Storm Simulator (CReSS). In particular, we consider six regions in northern Honshu (the largest island of Japan) as a test case. By applying the proposed index to simulated wind power, we show how the smoothing improves by distributing wind farms over different regions. Our results indicate that by distributing wind farms over only one to three regions, smoothing results vary considerably depending on the choice of regions. However, as the number of considered regions increases, the smoothing improves, and the particular choice of regions matters less for smoothing effects at the investigated timescales. This highlights the practical importance of deliberately selecting sites for large-scale wind power production to more effectively smooth the aggregated power.

Key Words: wind power, smoothing effect, Koopman mode, wind prediction, CReSS

Nonlinear Theory and Its Applications, IEICE, vol. 8, no. 4, pp. 342–357 DOI: 10.1587/nolta.8.342

1. Introduction

The continued increase of wind and solar power generation worldwide creates a necessity to understand the characteristics of aggregated power and in particular the reduced variability or *smoothing* achieved by dispersing the generation across a certain area. In this paper, we focus on wind power generation due to the unexploited potential, in particular for offshore installation, for which a rapid increase is expected within the next few years. Since wind is an intermittent and uncontrollable source of energy, and only a limited amount of electrical energy can practically be stored, one way of reducing variability in the aggregated power is to distribute the generation across a large area. The distribution of wind power raises questions regarding the characteristics and correlation between wind speed or power at different spatial and temporal scales, e.g. understanding the area size required to achieve a certain degree of smoothing [1]. A better understanding of the smoothing characteristics, i.e. reduction of fluctuations in the aggregated power, would intuitively facilitate smarter planning and better utilization of equipment and natural energy resources, as well as greater reliability [2]. Thus, when facing a future with a large share of wind and solar power in the commercial grid, a deliberate distribution of generation would benefit the forthcoming smart-grid development incorporating large-scale renewable energy generation.

In recent decades, smoothing effects of aggregated wind power have been addressed in numerous studies. Predominantly, various correlation analyses have been carried out, and frequency domain characteristics have been investigated via Power Spectral Density (PSD): see e.g. [3]. It was shown in [4] how the PSD of the total Wind Farm (WF) output is estimated via the PSD of the output of a single turbine, and the method showed good agreement with measurement data. Reduction of fluctuations in the aggregated power on an hourly scale was demonstrated in [5] for wind power dispersed over a large area (about 50×100 km in Germany) via second-order statistics and PSD. The reduction of variability in the aggregated power for WFs dispersed over a large area in Europe was also demonstrated in [1]. Based on a statistical analysis, it was concluded in [2] that the correlation between aggregated wind power in different geographical areas is similar to the correlation between WF outputs. In [6], wind power fluctuations were investigated by incorporating weather simulation data. The results showed that the timescales at which smoothing effects are achieved vary considerably between different geographical regions, and the authors concluded that regional wind characteristics need to be assessed in detail to estimate the smoothing effects of inter-regional wind power. In [7], correlations of hourly power variations in the Nordic countries (Sweden, Norway, Denmark, and Finland) were studied on distances up to 2000 km. It was shown how the cross-correlations of power depend on the time-averaging of the data, e.g. how correlation coefficients more drastically decrease with distance for 5-minutes (simply 5-min) averaged data in comparison to 1 h. It was shown in [8] that the PSD of wind power scales according to the so-called Kolmogorov spectrum as $S(f) \sim f^{-5/3}$. In [9], this characteristic was exploited by looking at the deviation from the Kolmogorov spectrum in the aggregated power as a measure of smoothing—since the non-aggregated power has been shown to follow it. The authors of [9] demonstrated an 87% reduction in wind power variability by interconnecting four WFs, and that interconnecting 16 more WFs only gave 8% additional reduction. In [10, 11], smoothing effects in a hypothetical WF and coherence between distant turbines were investigated via PSD, by using real measurements of wind speeds in Japan. A new index to quantify smoothing effects of wind power was proposed in [11], and the results from applying it indicated non-significant smoothing effects for periods longer than 100 min, for WFs located hundreds of kilometers apart.

This paper is a substantially enhanced version of our conference paper [12]. In the present paper, we newly propose and demonstrate a smoothing index of wind power based on spectral analysis via the so-called Koopman Mode Decomposition (KMD). KMD is a recently developed technique based on theory of the Koopman operator [13, 14] that governs the evolution of observables under an iteration of nonlinear dynamical systems. KMD and related methods have been applied successfully within the fields of fluid dynamics [15], power systems [16], and thermal dynamics in buildings [17]. Essentially, KMD derives a reduced system from dynamic data in terms of *modes*, i.e. spatial patterns oscillating with single frequencies for all observables (wind powers at hypothetical WFs in this paper). By

utilizing the phase and amplitude information of each observable which characterize the participation in each mode, we propose an averaged index of wind power smoothing via KMD, which follows previous investigations of wind power smoothing in Japan [10, 11] via PSDs. The performance of the proposed index is exemplified by incorporating large-scale weather simulation data from the Cloud Resolving Storm Simulator (CReSS) [18] to study practical smoothing effects of wind power in Japan. The used CReSS data have 1 h or 1 min temporal resolutions with 2 km spatial resolution. Smoothing has not extensively been investigated on a nationwide scale in Japan except for in [10, 11]. Because correlation of wind power has shown to vary significantly between geographical regions [1, 6], it is important to study every region specifically to acquire accurate knowledge necessary for planning purposes.

The contributions of this paper are twofold. First, based on the PSD-based smoothing index [11], we propose an index which is regarded as its generalization without any assumption on the spectrum of the data. We show through simple numerical examples that the proposed index indeed reproduces the same smoothing results if the assumptions for the PSD-based index hold. If they do not hold, the proposed index produces a slightly different result than the PSD-based one. Second, we utilize weather simulation data from CReSS to demonstrate the effectiveness of the proposed index. Through the use of CReSS data and the proposed index, we gain a new insight into the smoothing effects of wind power in Japan. We look at a test case with hypothetical WFs around a few sites in Japan where there are currently offshore wind power or construction projects exist. Considerable improvements in smoothing of aggregated power are observed for the case where two to three regions are utilized instead of a single one, whereas addition of more WF sites does not give significant additional improvement. Note, however, that these effects depend on the time-scale as well as the distance between WF sites.

The remainder of the paper is organized as follows. Section 2 describes a smoothing index calculated via PSDs, used as a comparison to the KMD-based index presented in this paper. Section 3 explains KMD briefly and derives the KMD-based smoothing index which we propose in this paper. In Section 4, we elaborate on the practical range of the smoothing index, and compare the KMD- and PSD-based indexes via simple numerical examples. Section 5 first briefly describes the weather simulation data from CReSS, and then presents the experimental results by applying the proposed index to data on wind power in Japan. Finally, we conclude the paper in Section 6.

2. Conventional smoothing index via power spectral densities

Smoothing of wind power in the frequency domain has conventionally been described by means of PSD [3, 5, 10]. This is a natural approach since integration of the PSD $S(f)$ of a signal in the frequency domain is equivalent to its variance σ^2:

$$\int_0^\infty S(f)\mathrm{d}f = \sigma^2. \tag{1}$$

Here, we are interested in quantifying the amount of smoothing achieved at a WF or in the aggregated power of multiple WFs. Now, let us denote the output power of a turbine or farm i by P_i and its PSD by $S_i(f)$. The aggregated power at a time t becomes $P_{\mathrm{tot}}(t) = \sum_{i=1}^m P_i(t)$, the normalized power $P^{\mathrm{n}}_{\mathrm{tot}}(t) = P_{\mathrm{tot}}(t)/m$ (n stands for *normalized*, and m is the number of WFs/turbines). Their PSDs are denoted by $S_{\mathrm{tot}}(f)$ and $S^{\mathrm{n}}_{\mathrm{tot}}(f)$, respectively. In [12], the following smoothing index was considered:

$$s_i(f) := \sqrt{S^{\mathrm{n}}_{\mathrm{tot}}(f)/S_i(f)}, \tag{2}$$

where $S_i(f)$ represents the PSD of "a typical" turbine/WF, which e.g. can be thought of as the turbine in a WF with a typical output. This is a measure of how much the total power fluctuates for a certain frequency f compared to "a typical" turbine/WF. When output powers and locations vary significantly, it becomes difficult to judge the correctness of such an index because of the difficulty determining "the typical" turbine/WF. Thus, the following different index was proposed in [12]:

$$s(f) := \underset{i}{\mathtt{tmean}}(s_i(f)), \tag{3}$$

where `tmean` represents the 25% truncated mean over all indexes $i = 1, \ldots, m$, to disregard the results of the most extreme spectra (outliers). We call this the *mean smoothing index via PSDs*, since it involves the truncated mean operation.

In this paper, we look at another index as a comparison to the index that we will propose later in this paper. First, the total power S_{tot} is given in [11] as follows:

$$S_{\mathrm{tot}}(f) = \sum_{i=1}^{m} S_i(f) + \sum_{i=1}^{m} \sum_{\substack{j=1 \\ j \neq i}}^{m} \sqrt{S_i(f) S_j(f)} \cdot \gamma_{ij}(f) \cos(\phi_{ij}(f)), \tag{4}$$

where $\gamma_{ij}(f) = |S_{ij}(f)| / \sqrt{S_i(f) S_j(f)}$ is the magnitude of coherence, and $\phi_{ij}(f) = \arg(S_{ij}(f))$ the phase between i and j, where $S_{ij}(f)$ is the cross-spectral density between P_i and P_j. Thus, we can understand that the amount of smoothing is highly dependent on the coherency, including the phase differences between individual powers constituting the aggregated power. Then, the following smoothing index is defined as in [11]:

$$\mathrm{coh}_{\mathrm{PSD}}(f) = \frac{1}{m(m-1)} \sum_{i=1}^{m} \sum_{\substack{j=1 \\ j \neq i}}^{m} \gamma_{ij}(f) \cos(\phi_{ij}(f)), \tag{5}$$

where it has been assumed that the PSDs of power at different locations are *identical*: see [11] for the detailed derivation. We call this the *averaged smoothing index via PSDs*, since it sums the coherence between any two locations, and then takes the average. With this index as a starting-point, we propose a new index in the next section.

3. New smoothing index via Koopman modes

In this section, we will directly state the decomposition celled the Koopman Mode Decomposition (KMD) without further theoretical elaborations. Derivations and theory can be found in numerous papers, e.g. [13–16, 19]. Following the definition, we introduce two smoothing indexes, where the one called the *averaged smoothing index via KMD* will be used later to evaluate smoothing effects of wind power in northern Japan. The index is regarded as a generalization of the previously proposed smoothing index calculated via PSDs.

3.1 Koopman mode decomposition

Consider $N+1$ vector-valued temporal snapshots of wind power measurements in the per unit (p.u.) system (power/(rated power)) collected at m locations: $\{\boldsymbol{P}_0, \ldots, \boldsymbol{P}_N\}$, $\boldsymbol{P}_k \in \mathbb{R}^m$, where k denotes a specific time-instance. The sampled data are then decomposed into a finite sum via KMD:

$$\left.\begin{aligned} \boldsymbol{P}_k &= \sum_{i=1}^{N} \tilde{\lambda}_i^k \tilde{\boldsymbol{v}}_i, \quad k = 0, \ldots, N-1, \\ \boldsymbol{P}_N &= \sum_{i=1}^{N} \tilde{\lambda}_i^N \tilde{\boldsymbol{v}}_i + \boldsymbol{r}. \end{aligned}\right\} \tag{6}$$

Above, they are computed via the Arnoldi-type algorithm [15] that outputs N pairs of the so-called Ritz-values $\tilde{\lambda}_i \in \mathbb{C}$ and Ritz-vectors $\tilde{\boldsymbol{v}}_i \in \mathbb{C}^m$. The vector $\boldsymbol{r}$ is called the residual in [15], and if it is assumed to be *zero*, (6) becomes

$$\boldsymbol{P}_k = \sum_{i=1}^{N} \tilde{\lambda}_i^k \tilde{\boldsymbol{v}}_i, \quad k = 0, \ldots, N. \tag{7}$$

Modal frequencies are calculated according to $f_i = \mathrm{Im}(\ln(\tilde{\lambda}_i))/(2\pi T_{\mathrm{s}})$, where T_{s} is the sampling period. The vector $\tilde{\boldsymbol{v}}_i = \boldsymbol{A}_i \angle \boldsymbol{\alpha}_i := [A_{i1}\angle\alpha_{i1}, A_{i2}\angle\alpha_{i2}, \ldots, A_{im}\angle\alpha_{im}]^\top$ ($\top$ denotes the transpose operation) is here called the *Koopman Mode* (KM) oscillating with the frequency f_i and contains

the magnitudes A_{ij} and phases α_{ij} of power fluctuations corresponding to the m measurements; e.g. outputs of m WFs. To identify lightly damped or undamped oscillations with large magnitude, all N KMs are sorted by $(\tilde{\lambda}_i)^N\|\tilde{\boldsymbol{v}}_i\|$, where $\|\cdot\|$ denotes the euclidean norm, and higher ranked ones are called *dominant* KMs, which are here used to evaluate smoothing effects.

3.2 New smoothing index

KMD will be applied to wind powers at m locations that represent hypothetical WFs. The total (aggregated) power $P_{\mathrm{tot},k}$ can be expressed using (7) as

$$P_{\mathrm{tot},k} = \boldsymbol{P}_k^\top \mathbf{1}_m = \sum_{i=1}^{N} \tilde{\lambda}_i^k \sum_{j=1}^{m} [\tilde{\boldsymbol{v}}_i]_j =: \sum_{i=1}^{N} \tilde{\lambda}_i^k \overline{\boldsymbol{v}}_i, \tag{8}$$

where $\boldsymbol{P}_k \in \mathbb{R}^m$ contains the measured powers at time k, $\mathbf{1}_m$ is the m-length vector of ones, $[\tilde{\boldsymbol{v}}_i]_j$ is the j-th component of $\tilde{\boldsymbol{v}}_i$, and $\overline{\boldsymbol{v}}_i \in \mathbb{C}$ is the scalar KM of the total power. That is, a spectral decomposition of the total power is achieved by applying KMD to individual outputs. Now, let $\overline{A}_i = |\overline{\boldsymbol{v}}_i|$ be the amplitude factor of the total power for the i-th KM, and analogously A_{ij} be the factor for the j-th output power. Then, following our previous work [12], we define

$$s_i := \frac{\overline{A}_i}{m \cdot \mathtt{tmean}(\boldsymbol{A}_i)}, \tag{9}$$

as a smoothing index, where $\boldsymbol{A}_i := [A_{i1}, \ldots, A_{im}]^\top$, and `tmean` is same as in (3). Note that m is included in (9) to scale the total output to WF p.u. If the amplitude factor $\overline{A}_i$ of the total power is smaller than the truncated mean of amplitudes for individual WFs contained in $\boldsymbol{A}_i$, then (9) becomes smaller than one, implying smoothing effect for the KM with frequency f_i. We call this the *mean smoothing index via KMD*. In addition to this index, we here introduce an index similar to (5):

$$\mathrm{coh}_{i,\mathrm{KMD}} = \frac{1}{m(m-1)} \sum_{j=1}^{m} \sum_{\substack{l=1 \\ l\neq j}}^{m} \hat{A}_{ij}\hat{A}_{il}\cos(\Phi_{jl}^i), \tag{10}$$

where $\Phi_{jl}^i := \alpha_{ij} - \alpha_{il}$, and $\hat{A}_{ij} := A_{ij}/\max(\boldsymbol{A}_i)$, i.e. components of $\boldsymbol{A}_i$ normalized by the largest component: see Fig. 1 for an illustration. The subscript i refers to the i-th *dominant* KM oscillating with the frequency f_i. We call this the *averaged smoothing index via KMD*, and it can be regarded as a generalization of a previously proposed index [11] which was shown to be effective for quantifying smoothing effects in Japan. The index theoretically takes a value in $[-1, 1]$, where '-1' indicates perfect smoothing and '1' no smoothing; however, it approximately takes a value in $[0, 1]$ for the practical data in this paper. This is because, first of all, '-1' is only achievable in the case of *two* signals in antiphase, but here we consider outputs at multiple locations. When the number of locations increases, the value indicating perfect smoothing approaches zero, which is shown in the

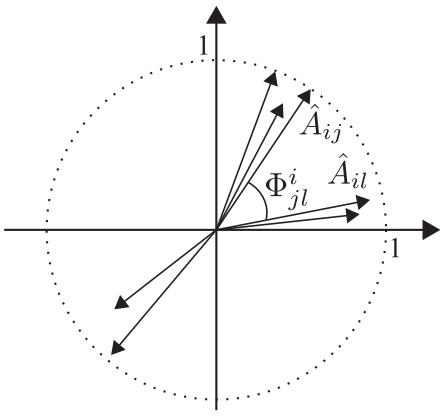

Fig. 1. Illustration of amplitudes and phases of KMs.

following section. Secondly, perfect smoothing of wind power is achieved for a large number of outputs with uncorrelated fluctuations or turbulence [3], whereas the number is not significantly large in this paper. For these reasons, a maximum achievable value of smoothing close to zero can be expected. Also, the proposed index (10) is not limited to the algorithm used to approximate KMD in this paper and can be computed with any technique producing a decomposition of the same type as (6) or (7). In fact, there are several different KMD algorithms proposed in literature: see e.g. [20, 21]. In addition, the index takes the same form as (5), which follows naturally from the notion and definition of coherency in KMs [19, 22], and does not rely on the assumptions used to derive (5). Thus, we can state that the KMD-based index (10) is regarded as a generalization of the PSD-based index (5), which is numerically demonstrated in the next section with simple examples.

4. Simple examples for comparison between smoothing indexes

Here, we first look at properties of the formula used to calculate the averaged smoothing via both KMD and PSDs, and second look at two simple numerical examples to clarify the similarities and differences between the two methods.

By dropping the index i in (10) and f in (5), and only considering a single frequency for simplicity, we rewrite the average coherence on a common form:

$$\mathrm{coh} = \frac{1}{m(m-1)} \sum_{j=1}^{m} \sum_{\substack{l=1 \\ l \neq j}}^{m} I_j I_l \cos(\theta_j - \theta_l), \quad m > 1, \tag{11}$$

where $I_j \angle \theta_j = \hat{A}_j \angle \alpha_j$ for KMD, or $I_j I_l \cos(\theta_j - \theta_l) = \gamma_{jl} \cos(\phi_{jl})$ for PSDs. Now, we think $I_i \angle \theta_i$ as a phasor as shown in Fig. 1 for KMD. The value '-1' on perfect smoothing is achieved when $m = 2$, $I_j = I_l = 1$, and $(\theta_j - \theta_l) = z\pi$ ($z \in \mathbb{Z}$). Thus, we consider a case where $m = 2n$ ($n \in \mathbb{N} > 1$) and $I_i = 1$ for all i, and we let $\theta_i = \beta$ ($i = 1, \ldots, m/2$) and $\theta_i = \beta \pm \pi$ ($i = m/2 + 1, \ldots, m$), where β is an arbitrary angle. This case implies two groups of unit-length phasors in anti-phase, hence perfect smoothing is achieved. In this case, (11) is simplified as

$$\mathrm{coh} = -\frac{m}{m(m-1)} = -\frac{1}{m-1}, \quad m > 1, \tag{12}$$

which goes to zero as m approaches infinity. Note that when m is not even as in the previous example, by letting e.g. $\theta_i = \beta$ ($i = 1, \ldots, \mathtt{floor}(m/2)$) and $\theta_i = \beta \pm \pi$ ($i = \mathtt{floor}(m/2)+1, \ldots, m$), i.e. allowing a difference of one between the number of anti- and in-phase phasors, (12) will closely approximate the smoothing in particular for "large" m. Note that the `floor` function (here we use MATLAB) takes the integer part of a value: e.g. $\mathtt{floor}(3/2) = 1$. Still, we consider two groups of phasors of unit lengths in anti-phase, denote the number of phasors in each group by m_1 and m_2 satisfying $m_1 + m_2 = m$, and the imbalance $\Delta m = |m_1 - m_2|$. Then, (11) can be simplified as

$$\mathrm{coh} = -\frac{m - (\Delta m)^2}{m(m-1)}, \quad 0 \leq \Delta m \leq m. \tag{13}$$

Here, (13) is equivalent to (12) for $\Delta m = 0$ (perfect smoothing) and becomes one for $\Delta m = m$ (i.e. no smoothing for only in-phase phasors). In Fig. 2, we have evaluated (13) for different m and Δm. The figure shows that for m as low as 10, values on smoothing close to zero are achieved for perfect smoothing ($\Delta m = 0$.) However, results as ideal as in the case of two anti-phase groups of phasors of equal lengths may be unrealistic for our practical data. Also, m is always larger than two for the wind power data in this paper. Thus, we say that the index approximately takes a value in the interval $[0, 1]$, although small negative values are sometimes observed in this paper.

Now, we look at simple numerical examples to clarify the differences and similarities between the KMD- and PSD-based averaged smoothing indexes. Let us consider the two signals given by

$$\begin{aligned} x_1(t) &= a_1 \cdot \sin(2\pi f_1 t) + b_1 \cdot \cos(2\pi f_2 t), \\ x_2(t) &= -\left\{ a_2 \cdot \sin(2\pi f_1 t + \varphi) + b_2 \cdot \cos\left(2\pi f_2 t - \frac{\pi}{3} + \varphi\right) \right\}, \end{aligned} \tag{14}$$

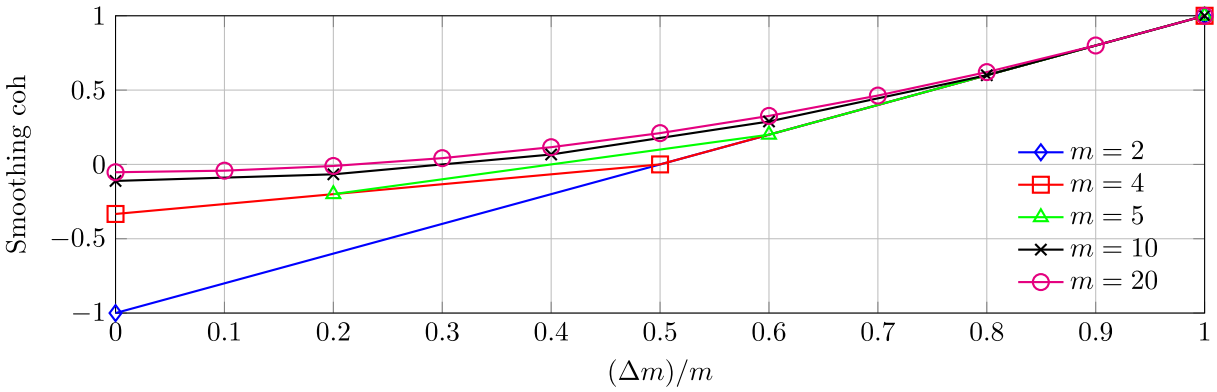

Fig. 2. Simplified smoothing index coh according to (13), evaluated for two groups of phasors of unit length in anti-phase for different m and Δm.

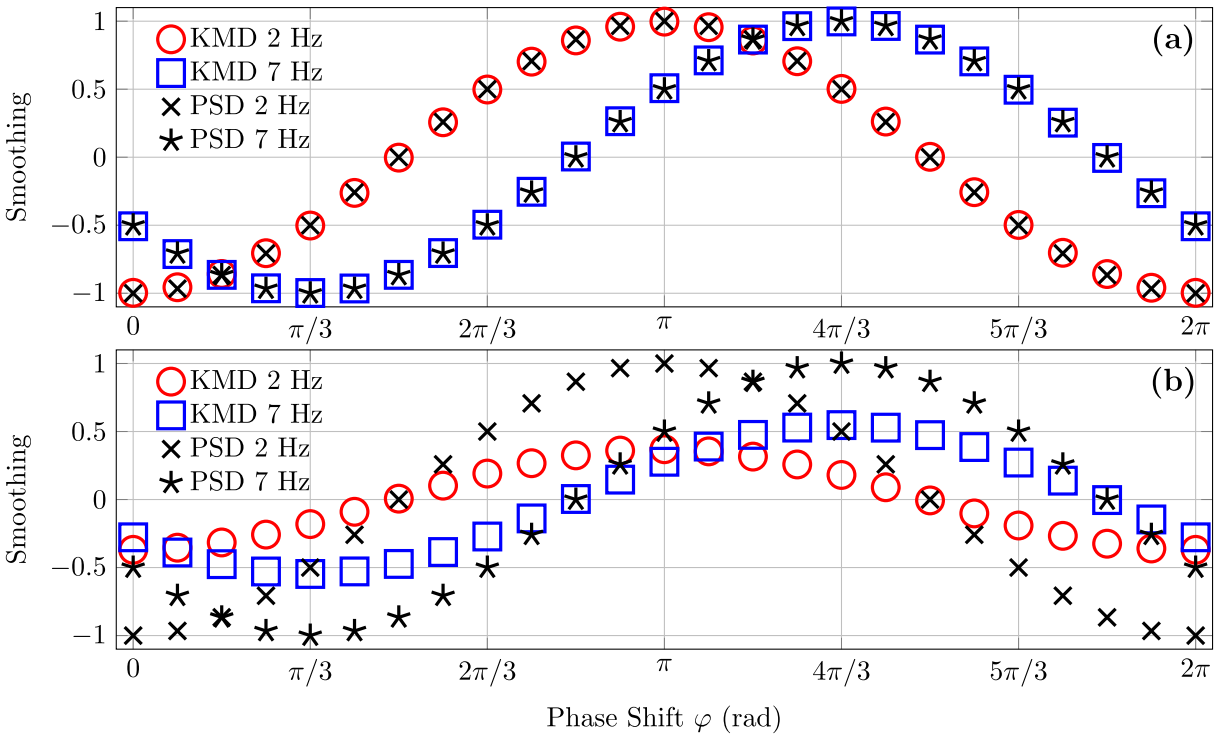

Fig. 3. KMD- and PSD-based averaged smoothing indexes applied to (14) under different phase shifts φ: For (a) Case 1; (b) Case 2.

where $f_1 = 2$ Hz and $f_2 = 7$ Hz. If $a_2 = a_1$ and $b_2 = b_1$, then perfect smoothing is achieved for 2 Hz if $\varphi = n2\pi$, and for 7 Hz if $\varphi = \pi/3 + n2\pi$, where $n \in \mathbb{N}$. Now, we vary φ between 0 and 2π, let the temporal length be 8 s ($N + 1 = 257$), and the sampling frequency $f_s = 32$ Hz. The MATLAB functions `cpsd` (cross-spectral density) and `mscohere` (magnitude squared coherence) are used to compute the PSD-based index (5) with no window overlap. The number of `fft` (fast Fourier transform) points is set at 128, and no window function such as Hamming is used.

Smoothing via the proposed (10) and the PSD-based index (5) is first computed for a case (Case 1) with $a_1 = a_2 = 0.8$, and $b_1 = b_2 = 0.6$. The results are shown in Fig. 3(a), and we see that the results become virtually identical for the two indexes. For example, when $\varphi = 0$, perfect smoothing is achieved for 2 Hz, which corresponds to a smoothing value of -1. In this case, the PSDs of $x_1(t)$ and $x_2(t)$ should be identical, and thus the derivation leading to the smoothing index (5) holds.

Now, let us consider (14) with $a_1 = 0.8$, $b_1 = 0.6$, $a_2 = 0.3$, and $b_2 = 1.1$ (Case 2). The smoothing results are given in Fig. 3(b). The PSD-based index here gives the same result as for Case 1, but the KMD-based index generates a slightly different result. The PSD-based index fails to quantify the smoothing correctly since it indicates perfect smoothing for a case where it is obviously impossible

because the amplitudes are not equal ($a_1 \neq a_2$, $b_1 \neq b_2$); also resulting in PSDs of different magnitudes. The proposed KMD-based index thus generalizes the PSD-based index for cases where the PSDs are not equal, which may be the case for the wind power data considered in this paper.

5. Numerical test with large-scale wind prediction data

Here we apply the proposed smoothing index (10) to simulated wind power data estimated using wind predictions with 1-h and 1-min time-resolutions. The 1-h data are from 36-h weather simulations, and the 1-min data are from a 30-h weather simulation.

5.1 Wind prediction data from CReSS

Data from the CReSS weather model [18] have been acquired including wind speeds in latitude, longitude and vertical directions; air pressure, and temperature for different heights z above sea level, e.g. $z = 10$ and 150 m: see Fig. 4 with $\Delta x = \Delta y = 2$ km.

Megawatt-rated turbines are mounted on about 100 m tall towers due to their long blades required to extract the energy. Because of this, the following equation is used to estimate wind speed at a height z [23]:

$$v_z = \frac{u_*}{k_v}\left[\ln\left(\frac{z-d}{z_0}\right) - \psi\right], \tag{15}$$

where k_v is the von Karman constant, u_* friction velocity, d displacement height, z_0 roughness length, and ψ a parameter taking the stability of the boundary layer into account, which here is assumed to be neutrally stable, implying $\psi = 0$. The parameters d and z_0 are dependent on the surface terrain, and d is assumed to be small compared to z and omitted, and z_0 is set to 2×10^{-4}, which is standard for open sea. By using the simplified $v_z = (u_*/k_v)\ln(z/z_0)$ and assuming equal friction velocities, the wind speed at a height z_2 from wind speed at z_1 can be approximated by

$$v_{z_2} = v_{z_1}\frac{\ln(z_2/z_0)}{\ln(z_1/z_0)}. \tag{16}$$

In this paper, using (16), we scale wind speed data at 10 m height to 80 m. We only consider the latitude and longitude components, and calculate the wind speed at 10 m height as $v_{10} = \sqrt{v_{x,10}^2 + v_{y,10}^2}$.

Two time series of wind speeds are shown in Figs. 5(a)–(b); one from the 1-h data and the other one from 1-min data. PSDs of the time-series are shown in Fig. 5(c). The PSD of wind power have been shown to follow the so-called Kolmogorov spectrum [8] according to $S(f) \sim f^{-5/3}$, and the spectrum of wind speed is similar [24]. The dashed line in the figure represent $c \cdot f^{-5/3}$, where c is a constant adjusted manually to match the PSDs. It is evident from these examples that the PSDs of wind speeds from CReSS scale according to Kolmogorov's theory, implying that wind speeds from CReSS have spectra close to real measured data.

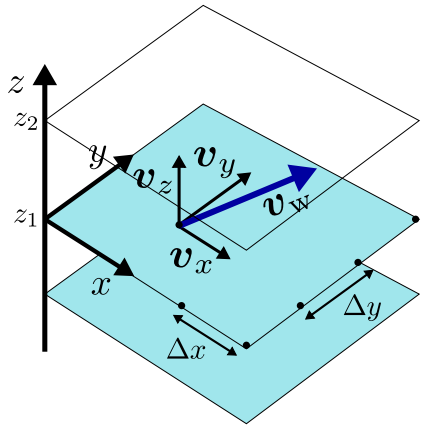

Fig. 4. Illustration of CReSS data.

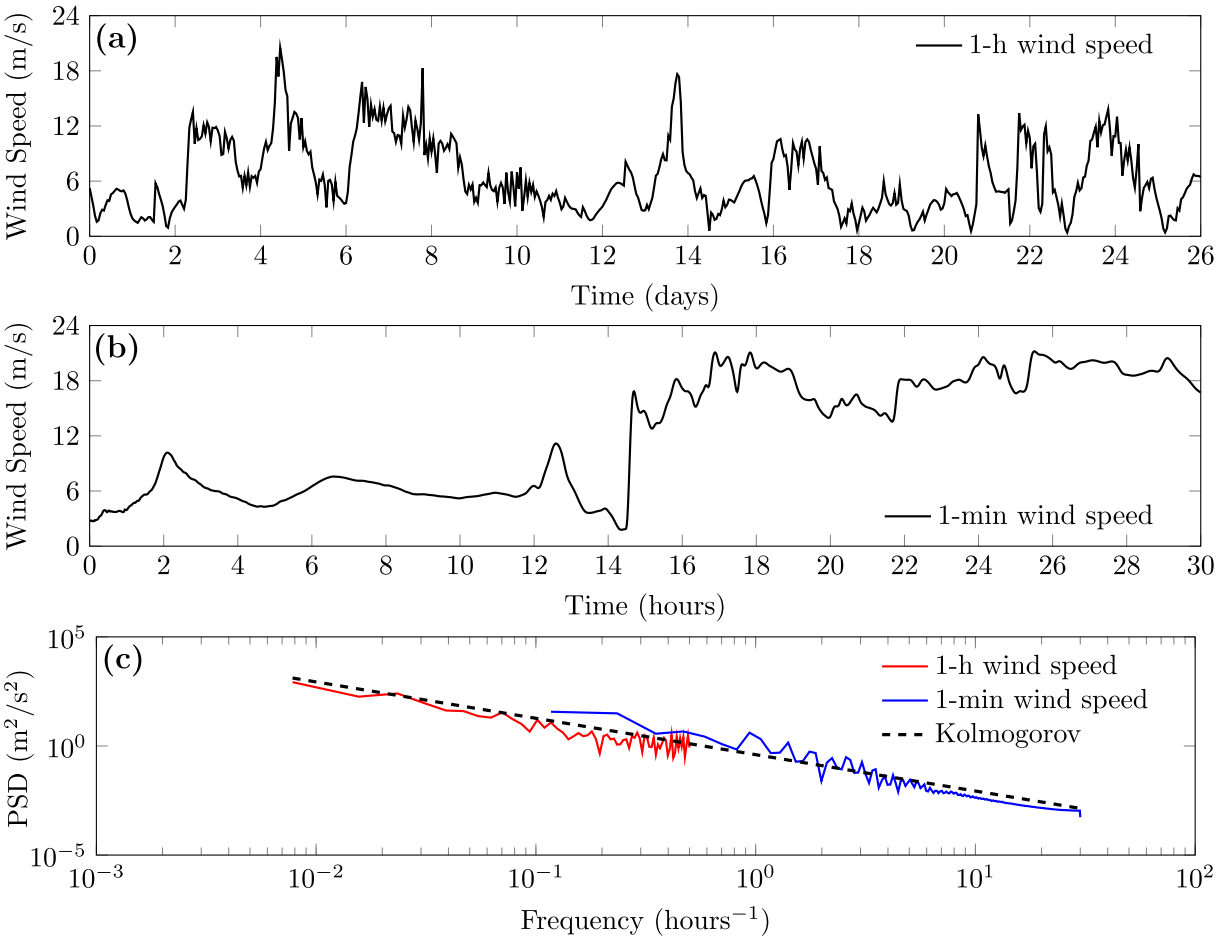

Fig. 5. Examples of (a) 1-h and, (b) 1-min wind speeds from CReSS, and (c) their Power Spectral Density (PSD) compared to Kolmogorov's spectrum.

5.2 Data sectioning and mean smoothing with KMD

For example, when applying the KMD-based smoothing index to 1-h sampled wind power predictions, we have a matrix of input data containing temporal snapshots collected over a month's period: $\mathsf{P}_{\text{in}} := [\boldsymbol{P}_1, \ldots, \boldsymbol{P}_{N_1}] \in \mathbb{R}^{m \times N_1}$; where m denotes the number of locations and N_1 the number of temporal snapshots. Here, we attempt to look at fluctuations of wind power on an hourly rather than daily scale due to their impact on power system operation [5, 25]. Because of this, we arrange the input data into sub-matrices P_i containing three days of wind speed data to have a reasonable amount of temporal snapshots in each matrix, each time-shifted L (e.g. one day) from the previous one, and define the input to KMD as

$$\mathsf{P}_{\text{new}} := \begin{bmatrix} \mathsf{P}_1 \\ \vdots \\ \mathsf{P}_p \end{bmatrix} \in \mathbb{R}^{(p \cdot m) \times N_2}, \tag{17}$$

where N_2 is the number of temporal snapshots in each sub-matrix P_i, and p the number of sub-matrices: see Fig. 6. Each sub-matrix $\mathsf{P}_i := [\boldsymbol{P}_{1+(i-1)L}, \ldots, \boldsymbol{P}_{N_2+(i-1)L}]$ can be seen as a subsection of data, and the observables, i.e. the m measurement locations are the same only time-shifted in each section. When applying the KMD-based averaged smoothing index, the smoothing is calculated for each section, and the total result is averaged over all sections. In this way, we obtain a result on smoothing which has been averaged over a month's duration. Long time-series of 1-min sampled wind power data are also treated in the same way with this type of sectioning.

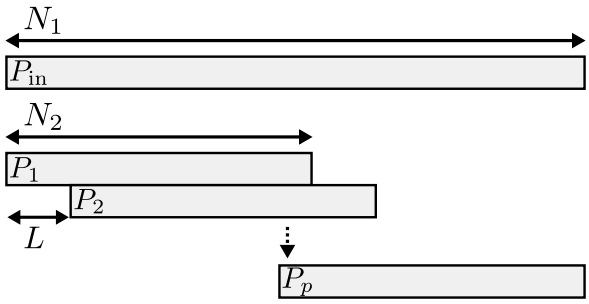

Fig. 6. Illustration of data sectioning used with KMD.

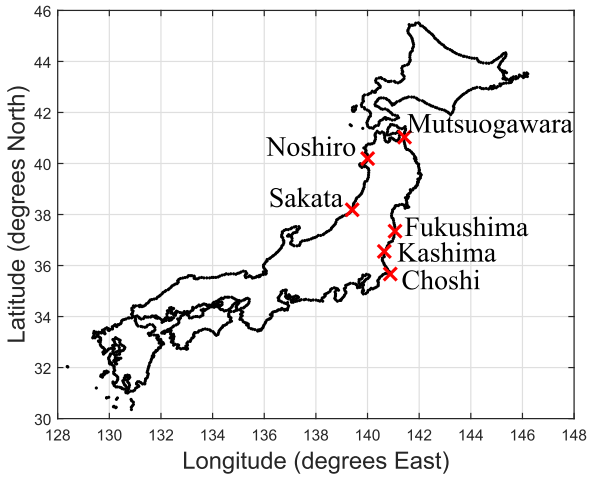

Fig. 7. Set of wind speed measurement points outlining the coasts of Japan's main islands, indicated by black dots. Red crosses roughly mark six regions in Northern Honshu, where there are WFs or project/plans: Mutsuogawara, Noshiro, Sakata, Fukushima, Kashima, and Choshi.

5.3 Smoothing of wind power in northern Honshu

In this section, we demonstrate the proposed smoothing index via KMD. Two types of data are used in the demonstration. The first type is daily wind predictions with 1-h time resolution which have been obtained for a period of 3.5 years. However, there are temporal gaps in the data, and hence we will look at months where data from many consecutive days are available. Here, we use data from December 2012 (26 days), February 2015 (28 days), and July 2014 (30 days). The second type is predictions with 1-min time-resolution and temporal length of 30 h, from January 2013.

We will look at wind power around six regions in Japan where there are offshore WFs, or ongoing projects. The six considered regions are shown in Fig. 7: Mutsuogawara, Noshiro, Sakata, Fukushima, Kashima, and Choshi. The WF outputs are approximated from wind speeds using a wind turbine power curve: see Fig. A-1(b) in the appendix.

First, we look at correlations between predicted wind speeds. The decrease in wind speed and wind power correlation with distance is similar and is often modeled by exponential functions [7, 26]. Figure 8 shows linear correlation coefficients of wind speeds along the coast of Honshu for both 1-h and minute time-resolution data. The 1-h data are from December 2012, but the results are similar for all months considered in this paper. The correlations are computed with respect to a reference point north of Noshiro (see Fig. 7), located along the Sea of Japan coast, close to the northernmost point of Honshu. In Fig. 8, we highlight locations along the Sea of Japan coast and the Pacific Coast in different colors. Significantly higher correlations are observed along the Sea of Japan coast, whereas correlations are lower for locations along the Pacific Coast. This difference in correlation is particularly apparent in Fig. 8(a) for the hourly data. A distinct outlier is noted, which may be an effect of the location deep within an inlet. For correlations of minute time-resolution data shown in Fig. 8(b), results for 10-min averages (from 1-min data) generally show increased correlation in comparison with 1-min data. The correlations decrease quickly towards zero and below (anti-correlation).

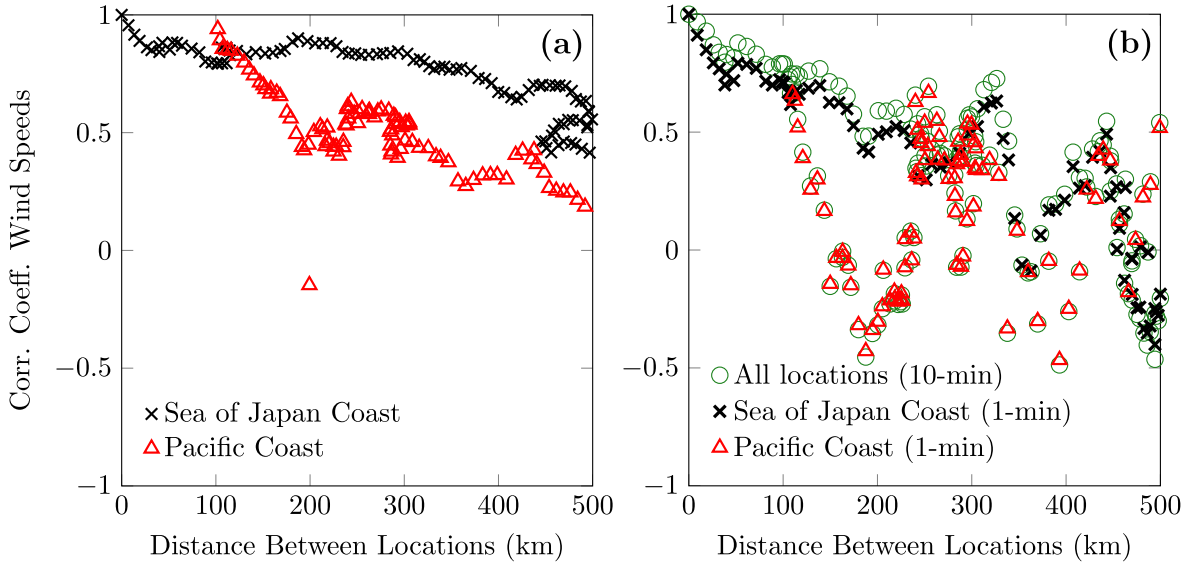

Fig. 8. Correlation coefficients of wind speeds along the coast of Honshu for (a) 1-h wind speeds; and (b) 1-min and 10-min averaged wind speeds.

The anti-correlations are likely an effect of the short time-period of the simulations (30 hours) and the weather characteristics on that particular day, and such effects are likely to disappear for longer time-series—since this is not observed with the hourly data which takes the macro-scale correlations on longer timescales into account. Negative correlations are rare between WFs [2], and [1] reports slightly negative correlations for long distances (1500–3000 km). The observed phenomenon should therefore be examined with more simulation data and real measurements.

5.3.1 Improved smoothing by dispersing wind farms

Now, we look at smoothing effects of aggregated wind power by applying the proposed averaged smoothing index via KMD. In Fig. 9(a), smoothing of aggregated wind power is shown for the December data as the number of WFs around Fukushima (see Fig. 7) varies from 4 to 20 in steps of 4. Initially, in Fig. 9(a), the smoothing improves when the number of WFs increases from 4 to 8. However, after this, smoothing does not seem to improve as rapidly with more WFs. Now, using the 1-min data, smoothing results are shown in Fig. 9(b) for input data with temporal length of 14 h, 4 h long sections, and 2 h overlap. As for the 1-h data, a pronounced improvement in smoothing is observed by increasing the number of WFs from 4 to 8, and after that only minor improvements are observed. Here, it should be noted that the 1-h and 1-min data come from different datasets with different dimensions and small differences in the geographical data, thus the positions are only roughly the same. The maximum distances between any two WFs for the cases of 4, 8, and 12 WFs for the 1-h data are 26, 62, and 94 km, and for the 1-min data they are 30, 66, and 105 km. The marked increase in smoothing from 4 to 8 WFs mainly comes from doubling the maximum distance, causing less coherence between WF outputs.

In Figs. 9(c)–(d), smoothing results for both 1-h and 1-min data are shown for the cases of placing one or two WFs in each of the six regions. The results are compared to the cases of 6 or 12 WFs around Fukushima. Figures 9(c) and (d) clearly show that the smoothing improves substantially when distributing WFs around the six regions in comparison with just one (Fukushima). The smoothing in the cases of 6 and 12 WFs become very similar when they are distributed equally between the regions. However, the smoothing differs more for 6 or 12 WFs around only Fukushima. Intuitively, we can expect this, because increasing the maximum distance between WFs from roughly 50 km for 6 WFs around Fukushima to 100 km for 12 WFs, i.e. a twofold increase, should improve the smoothing due to the decrease in correlation of wind speeds/powers. Nonetheless, even when increasing the number of WFs to 30 (maximum distance 210 km), the smoothing effects are not as good (but almost) as when utilizing six regions. Also, the addition of a second WF in each region a few kilometers away

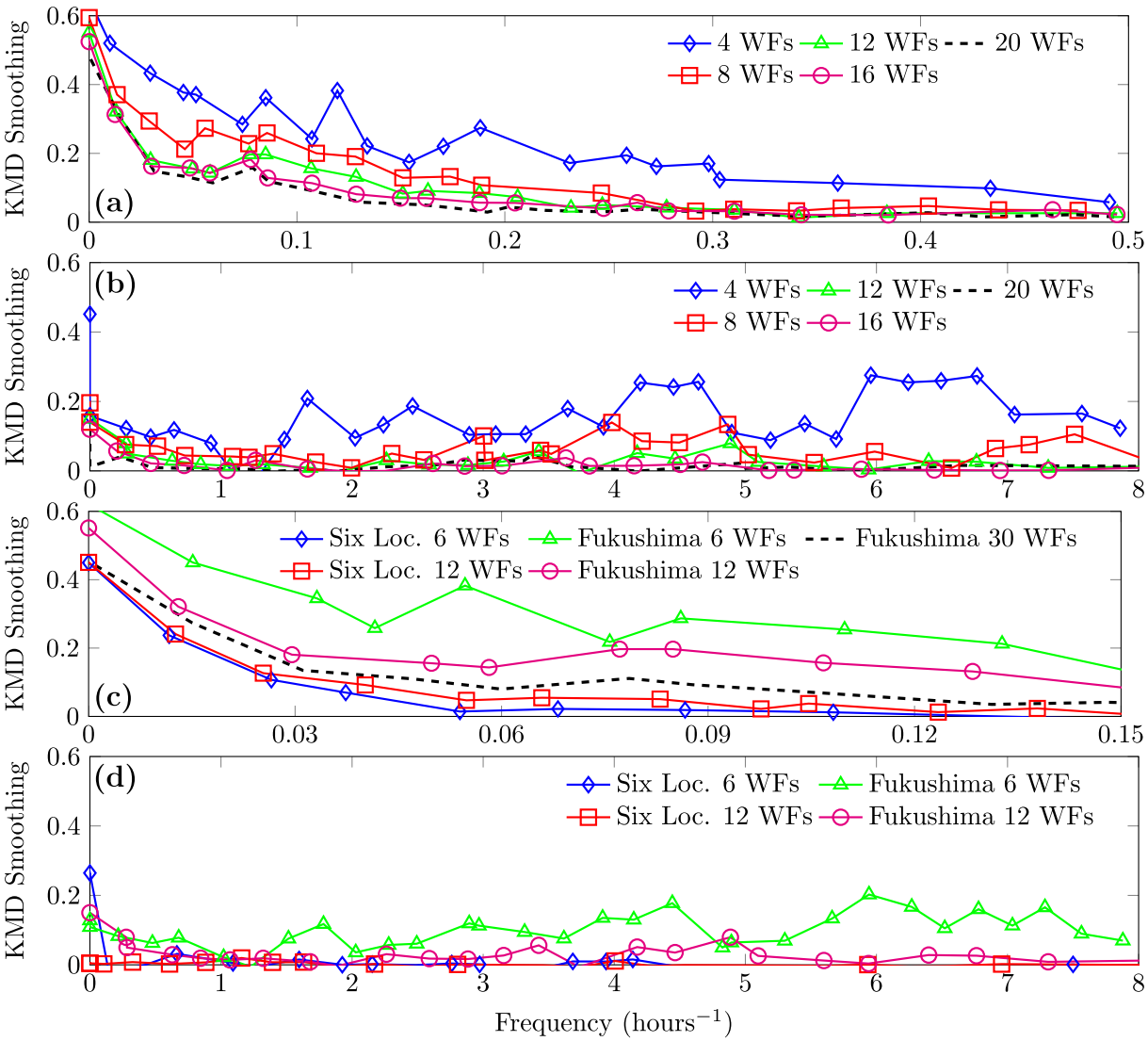

Fig. 9. Smoothing around Fukushima as the number of WFs vary from 4 to 24 for (a) 1-h wind prediction data from December 2012 as input and (b) 1-min data. Smoothing for 6 or 12 WFs in Fukushima and WFs distributed over the six regions (locations) shown in Fig. 7, for (c) 1-h wind prediction data from December 2012 as input and (d) 1-min data.

from the first one, did not have as pronounced effect when looking at this temporal (1 h and 1 min) and spatial (2 km) resolutions. Thus, the main origin of the observed improvement of smoothing observed is the vast distribution of WFs across northern Japan, which substantially decreases the correlation/coherence of wind power.

5.3.2 Smoothing dependence on the number and choice of regions

Here, we look at how smoothing depends on the number of geographical regions chosen among the ones indicated in Fig. 7, by looking at all combinations of l regions of the set of $n = 6$ considered regions. That is, we consider in total $\sum_{l=1}^{n} n!/((n-l)!l!) = 63$ cases. The total number of WFs is fixed at 12. For example, in the case of $l = 5$, there will be 2 WFs in four regions and 4 WFs in one region. In all other cases, the 12 WFs will be evenly distributed between the l regions. To quantify the smoothing in each case c, we consider the smoothing integrated over frequency: $\Sigma_c := \int_{f=0}^{f_\infty} s_c(f)\mathrm{d}f$, calculated with the trapezoidal method, where $s_c(f)$ ($f \in [0, f_{\infty,c}]$) represents the calculated smoothing from the KMD-based averaged smoothing index, and $f_\infty := \min([f_{\infty,1}, \ldots, f_{\infty,63}])$. Then, we look at the normalized smoothing defined by $\hat{\Sigma}_c := \Sigma_c / \max([\Sigma_1, \ldots, \Sigma_{63}])$, where the maximum Σ_c is naturally achieved for a case where $l = 1$ (one region), where we anticipate less smoothing since the correlation

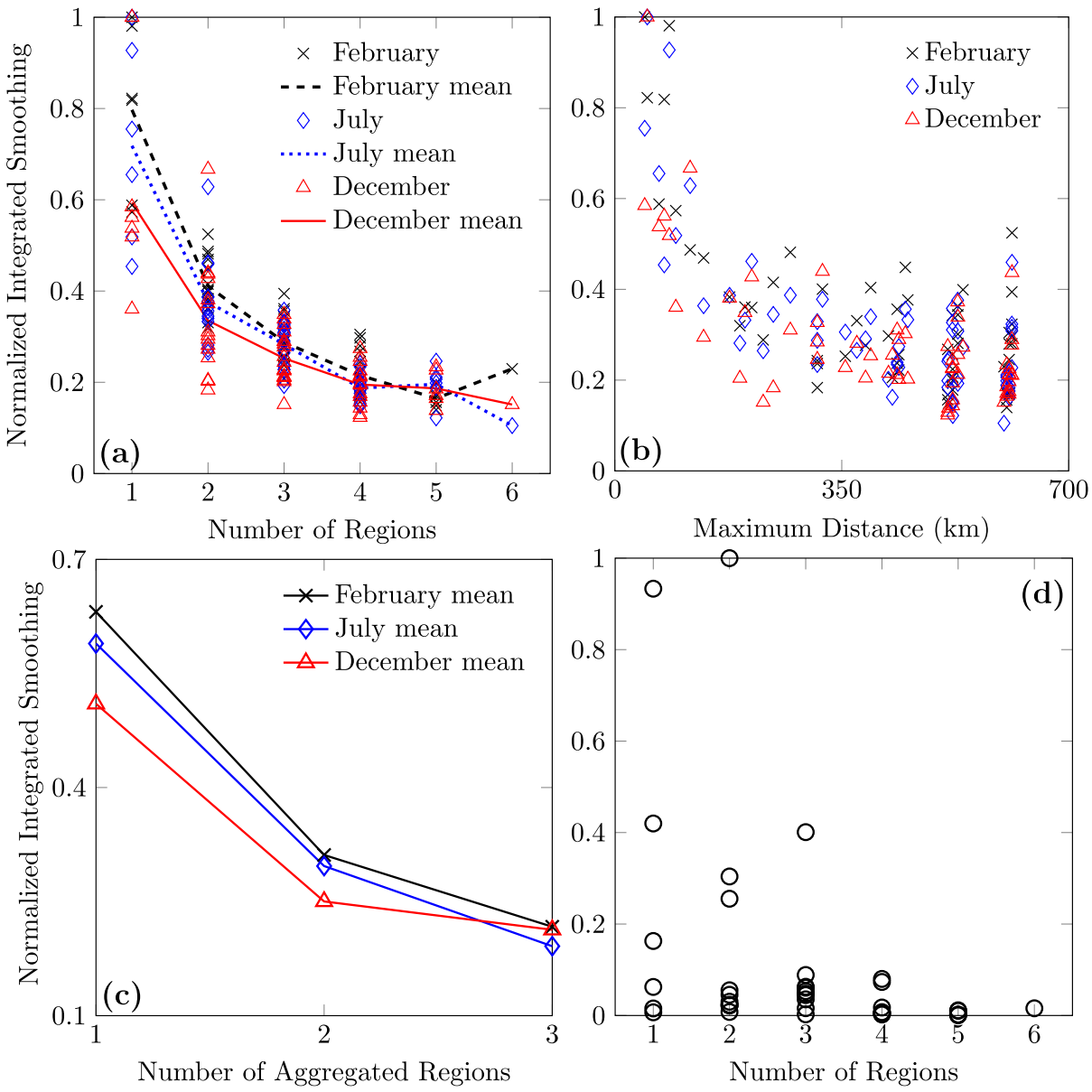

Fig. 10. Normalized integrated smoothing vs.: (a) the number of regions for 1-h data, and the mean results; (b) distance; (c) aggregated regions where the results have been averaged for each region; (d) number of regions for 1-min data.

of wind powers within a region is likely higher than between regions.

Results from calculating this "normalized integrated smoothing" plotted vs. the number of regions are shown in Fig. 10(a) for 1-h data of February, July, and December. Here, smaller improvements in smoothing are observed for a larger number of regions l, while the smoothing varies more for $l = 1, 2$, and 3. These results confirm the intuitive notion that the smoothing will depend highly on the particular regional characteristics when looking at only one or a couple of regions, while these characteristics tend to cancel out when looking at multiple regions. Note that the results for all months become close, which is clearly seen by looking at the mean results. The smoothing vs. maximum distance between WFs is shown in Fig. 10(b). A clear, exponential decrease in smoothing is observed with increased distance for all months. Exponential decrease in correlation with increased distance has been shown in numerous studies—see e.g. [2]—which is a likely cause of this. Our results indicate that increasing the maximum distance up to about 200 km improves the smoothing significantly, whereas further increments provide less noticeable improvements. Here, it should be noted that when the distance reaches about 200 km, smoothing results for inter-regional distributions

are included, such as WFs both at the west (Sea of Japan) and east (Pacific Ocean) coasts of Japan, whereas distances below about 200 km only include one region, or multiple "close" regions such as Kashima and Choshi. To more clearly illustrate the improvements in smoothing for inter-regional distribution of WFs, we reduce the number of regions to three very rough (aggregated) regions as follows: Mutsuogawara by itself in the north, Noshiro and Sakata along the Sea of Japan coast, and Fukushima, Kashima, and Choshi along the Pacific Coast. As an example, if all WFs are located around Noshiro and Sakata, the number of included aggregated regions only becomes one. In Fig. 10(c) we have plotted the mean smoothing results (using the same data as in Fig. 10(a)) vs. the number of aggregated regions. The results clearly indicate similar improvements for all months by dispersing the generation inter-regionally over at least two regions. The cause of this can be attributed to the different correlation characteristics that were discussed in Section 5.3.

The smoothing results for the 1-min data are shown in Fig. 10(d). These results differ significantly from the results using the 1-h wind data, in that much larger smoothing effects are observed overall. In fact, most of the cases yield smoothing close to zero, which indicates almost perfect smoothing. The result suggests that the distance between WFs in one or two regions only is enough to make the wind powers uncorrelated at this time-scale. The rapid decrease in correlation for smaller spatial and temporal scales was demonstrated in Fig. 8, and has been shown in e.g. [7].

6. Conclusions

In this paper, we proposed a new smoothing index of wind power based on the KMD, which decomposes the complex spatio-temporal data on wind power into modes oscillating with single frequencies. It was shown that the proposed smoothing index is regarded as a generalization of a previously proposed index based on power spectral densities. Our results from applying our proposed index to wind predictions from CReSS indicated that by distributing wind power across only one to three regions in Northern Japan, smoothing can vary considerably; and, as the number of regions increases, the particular choice of regions matters less. In particular, our results demonstrated that a distribution of WFs between the Sea of Japan coast and the Pacific Coast results in greater improvements in smoothing than WFs placed along the same coast. This highlights the practical importance of deliberately selecting regions for large-scale wind power production to more effectively smooth the aggregated power. Furthermore, an exponential-like improvement in smoothing with increasing distance was observed.

Several direct extensions of this work are possible. In this paper we mainly looked at 1-h data, while data of higher temporal resolution may be highly interesting for studies on short-term power system operation. It would also be important to cross-check the simulated wind speeds and power outputs against real measurements around Japan to verify their correctness. Applying the proposed index to real measured data is also of great practical importance. In the current paper, the applicability of the CReSS was briefly demonstrated for wind power analysis in Japan, but many additional studies incorporating CReSS-data are possible; to name a few: wind power prediction, economic dispatch with high penetration of wind power, and detailed case studies to evaluate potential WF locations.

Acknowledgments

This work was supported in part by MEXT KAKENHI #15H03964 and JST CREST #JPMJCR15K3.

References

[1] G. Giebel, "On the benefits of distributed generation of wind energy in Europe," Ph.D. thesis, University of Oldenburg, 2000.

[2] H. Louie, "Correlation and statistical characteristics of aggregate wind power in large transcontinental systems," *Wind Energy*, vol. 17, no. 6, pp. 793–810, 2014.

[3] J. Manwell, J. McGowan, and A. Rogers, *Wind Energy Explained: Theory, Design and Application*, Wiley, 2009.

[4] G. McNerney and R. Richardson, "The statistical smoothing of power delivered to utilities by multiple wind turbines," *IEEE Transactions on Energy Conversion*, vol. 7, no. 4, pp. 644–647, 1992.

[5] H.G. Beyer, J. Luther, and R. Steinberger-Willms, "Power fluctuations in spatially dispersed wind turbine systems," *Solar Energy*, vol. 50, no. 4, pp. 297–305, 1993.
[6] B. Tarroja, F. Mueller, J.D. Eichman, J. Brouwer, and S. Samuelsen, "Spatial and temporal analysis of electric wind generation intermittency and dynamics," *Renewable Energy*, vol. 36, no. 12, pp. 3424–3432, 2011.
[7] H. Holttinen, "Hourly wind power variations in the Nordic countries," *Wind Energy*, vol. 8, no. 2, pp. 173–195, 2005.
[8] J. Apt, "The spectrum of power from wind turbines," *Journal of Power Sources*, vol. 169, no. 2, pp. 369–374, 2007.
[9] W. Katzenstein, E. Fertig, and J. Apt, "The variability of interconnected wind plants," *Energy Policy*, vol. 38, no. 8, pp. 4400–4410, 2010.
[10] T. Nanahara, M. Asari, T. Sato, K. Yamaguchi, M. Shibata, and T. Maejima, "Smoothing effects of distributed wind turbines. Part 1. Coherence and smoothing effects at a wind farm," *Wind Energy*, vol. 7, no. 2, pp. 61–74, 2004.
[11] T. Nanahara, M. Asari, T. Sato, K. Yamaguchi, M. Shibata, and T. Maejima, "Smoothing effects of distributed wind turbines. Part 2. Coherence among power output of distant wind turbines," *Wind Energy*, vol. 7, no. 2, pp. 75–85, 2004.
[12] F. Raak, Y. Susuki, K. Tsuboki, M. Kato, and T. Hikihara, "On smoothing effects of wind power via Koopman mode decomposition," *NOLTA2016*, Yugawara, Japan, pp. 366–369, 2016.
[13] I. Mezić, "Spectral properties of dynamical systems, model reduction and decompositions," *Nonlinear Dynamics*, vol. 41, no. 1-3, pp. 309–325, 2005.
[14] I. Mezić, "Analysis of fluid flows via spectral properties of the Koopman operator," *Annual Review of Fluid Mechanics*, vol. 45, pp. 357–378, 2013.
[15] C.W. Rowley, I. Mezić, S. Bagheri, P. Schlatter, and D.S. Henningson, "Spectral analysis of nonlinear flows," *Journal of Fluid Mechanics*, vol. 641, pp. 115–127, 2009.
[16] Y. Susuki, I. Mezic, F. Raak, and T. Hikihara, "Applied Koopman operator theory for power systems technology," *NOLTA*, vol. 7, no. 4, pp. 430–459, 2016.
[17] M. Georgescu and I. Mezić, "Building energy modeling: A systematic approach to zoning and model reduction using Koopman mode analysis," *Energy and Buildings*, vol. 86, pp. 794–802, 2015.
[18] K. Tsuboki, "High-resolution simulations of high-impact weather systems using the cloud-resolving model on the Earth Simulator," in *High Resolution Numerical Modelling of the Atmosphere and Ocean*, pp. 141–156, Springer, 2008.
[19] M. Budišić, R. Mohr, and I. Mezić, "Applied Koopmanism," *Chaos*, vol. 22, no. 4, p.047510, 2012.
[20] Y. Susuki and I. Mezić, "A Prony approximation of Koopman mode decomposition," *2015 IEEE 54th Annual Conference on Decision and Control (CDC)*, pp. 7022–7027, December 2015.
[21] K.K. Chen, J.H. Tu, and C.W. Rowley, "Variants of dynamic mode decomposition: Boundary condition, Koopman, and Fourier analyses," *Journal of Nonlinear Science*, vol. 22, no. 6, pp. 887–915, 2012.
[22] Y. Susuki and I. Mezić, "Nonlinear Koopman modes and coherency identification of coupled swing dynamics," *IEEE Transactions on Power Systems*, vol. 26, no. 4, pp. 1894–1904, 2011.
[23] U.B. Gunturu and C.A. Schlosser, "Characterization of wind power resource in the United States," *Atmospheric Chemistry and Physics*, vol. 12, no. 20, pp. 9687–9702, 2012.
[24] P. Milan, M. Wächter, and J. Peinke, "Turbulent character of wind energy," *Physical Review Letters*, vol. 110, no. 13, p.138701, 2013.
[25] Y.H. Wan, M. Milligan, and B. Parsons, "Output power correlation between adjacent wind power plants," *Journal of Solar Energy Engineering*, vol. 125, no. 4, pp. 551–555, 2003.
[26] C. St. Martin, J. Lundquist, and M. Handschy, "Variability of interconnected wind plants: Correlation length and its dependence on variability time scale," *Environmental Research Letters*, vol. 10, no. 4, 2015.
[27] K. Elkington, J.G.H. Slootweg, M. Ghandhari, and W.L. Kling, "Reduced-order modelling of

wind turbines," in *Wind Power in Power Systems*, ed. T. Ackermann, pp. 821–847, John Wiley & Sons, 2012.

[28] J.G. Slootweg, S.W.H. de Haan, H. Polinder, and W.L. Kling, "General model for representing variable speed wind turbines in power system dynamics simulations," *IEEE Transactions on Power Systems*, vol. 18, no. 1, pp. 144–151, 2003.

Appendix

A. Wind power conversion model

The power extracted from wind is given in [27] as

$$P_{\mathrm{w}} = \frac{1}{2}\rho c_{\mathrm{p}}(\lambda,\beta)A_{\mathrm{r}}v_{\mathrm{w}}^3, \tag{A-1}$$

where ρ is the air density (here 1.225 kg/m^3), c_{p} the power coefficient which is a function of tip speed ratio λ and pitch angle β ($\beta \geq 0°$), $A_{\mathrm{r}} = \pi r^2$ the area swept by the rotor blades with length r (m), and v_{w} wind speed (m/s). The power coefficient c_{p} is modeled as in [27, 28]:

$$c_{\mathrm{p}} = c_1\left(\frac{c_2}{\lambda_{\mathrm{i}}} - c_3\beta - c_4\beta^{c_5} - c_6\right)\exp\left(-\frac{c_7}{\lambda_{\mathrm{i}}}\right), \tag{A-2}$$

with λ_{i} defined as

$$\frac{1}{\lambda_{\mathrm{i}}} = \frac{1}{\lambda + c_8\beta} - \frac{c_9}{\beta^3 + 1}. \tag{A-3}$$

The tip speed ratio is defined as $\lambda := v_{\mathrm{bt}}/v_{\mathrm{w}} = (\omega_{\mathrm{t}} r)/v_{\mathrm{w}}$, where v_{bt} is the speed of the turbine blades, and ω_{t} (rad/s) is the mechanical angular velocity of the turbine rotor.

An optimal relation between P_{w} and ω_{t}, $P_{\mathrm{w}}^*(\omega_{\mathrm{t}})$ is derived by tracking the maximum value of (A-1) for different wind/rotor speeds, called maximum power point tracking: see Fig. A-1(a). $P_{\mathrm{w}}^*(\omega_{\mathrm{t}})$ is used to control the turbine at optimal power. The power curve $P_w(v_{\mathrm{w}})$ is now derived by solving

$$P_{\mathrm{w}}(\lambda(v_{\mathrm{w}},\omega_{\mathrm{t}})) - P_{\mathrm{w}}^*(\omega_{\mathrm{t}}) = 0, \tag{A-4}$$

for a number of wind speeds v_{w}, and shown in Fig. A-1(b).

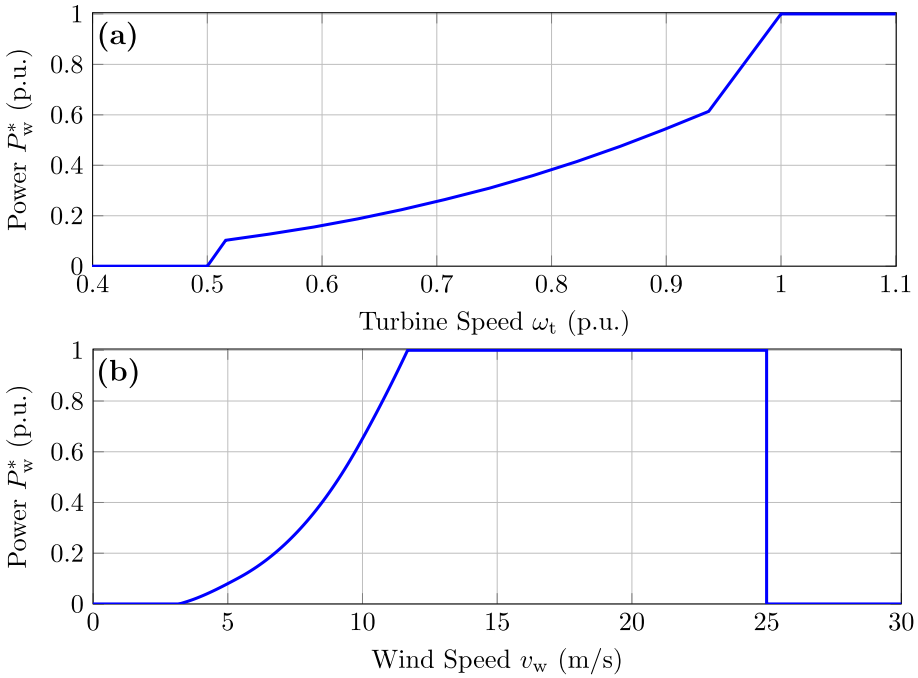

Fig. A-1. Optimal power vs. speed curve in (a) and derived power curve in (b) utilized in this paper.